State space modelling of variation propagation in multistage machining processes for variable stiffness structure workpieces

Kun Wang, Guilong Li, Shichang Du, Lifeng Xi & Tangbin Xia

Published online: 04 May 2020.

State space modelling of variation propagation in multistage machining processes for variable stiffness structure workpieces

Kun Wang[a], Guilong Li[a], Shichang Du[a,b*], Lifeng Xi[a,b] and Tangbin Xia[a,b]

[a]*Department of Industrial Engineering and Management, School of Mechanical Engineering, Shanghai Jiao Tong University, Shanghai, People's Republic of China;* [b]*State Key Lab of Mechanical System and Vibration, Shanghai Jiao Tong University, Shanghai, People's Republic of China*

Satisfying the quality requirement of products in multistage machining processes (MMPs) is significant and challenging nowadays. In spite of the success of the stream of variation (SoV) theory in variation propagation modelling for MMPs, the absence of elastic deformation variations could be an important factor that limits its application in variable stiffness structure (VSS) workpieces. To this end, a generic variation propagation framework in MMPs for VSS workpieces is established, incorporating the induction and propagation of elastic deformation variations. Region division strategy is adopted according to the characteristics of VSS workpieces, and the analytic solutions of elastic deformation in different regions are solved by contact theory and elastic theory. The effectiveness and accuracy of the proposed model are verified by a six-stage machining process on a four-cylinder engine block, and the proposed model is compared with the conventional SoV model resulting in a significant improvement on quality prediction.

Keywords: Multistage machining processes; variation propagation modelling; variable stiffness structure; elastic deformation

1. Introduction

Multistage machining processes (MMPs) are widely adopted in manufacturing industry to obtain a high-quality product by removing materials from a rough-cast. Satisfying dimensional and geometric precision of key product characteristics (KPCs) from MMPs is significant, yet challenging nowadays (Shi 2006). For a particular stage, quality features deviate from designed target values due to imperfections on fixture locators and variations during machining. If some of these deviating features are adopted as datum features at downstream stages, their deviations will be propagated and accumulated, which will finally affect the machining accuracy of KPCs (Duan and Wang 2013; Arizono, Yoshimoto, and Tomohiro 2020). Since the deviation analysis of KPCs is of great concern in quality grading (Yanıkoğlu and Denizel 2020), manufacturing system monitoring (Du et al. 2015) and preventive maintenance integration (Rezaei-Malek et al. 2019a; Zhao et al. 2020), it is desirable to develop a mathematical model that explicitly describes the intrinsic variation induction and propagation in MMPs. In existing researches, the most commonly used methods are the Markov modelling and the theory of stream of variation (SoV).

The basis of the Markov model is the 'no memory' Markov chain. The feature is similar to the multistage process, i.e. the random variable only depends on its previous value. Therefore, some scholars used the Markov method in MMPs (Du et al. 2015; Behnamian et al. 2017; Liu, Du, and Xi 2018; Jia and Zhang 2019). However, this method can only give the qualified probability of the characteristics, which is relatively rough for the accurate solution of KPC deviations. The theory of SoV reveals the mapping relationship between key control characteristics (KCCs) and KPCs and it is an effective method in researching variation propagation rules of MMPs (Shi 2006). Since Hu and Koren (1997) firstly proposed this theory in automobile assembly, the SoV model for multistage assembly processes (MAPs) has received extensive attention (Jin and Shi 1999; Mantripragada and Whitney 1999; Guo et al. 2016; Genta, Galetto, and Franceschini 2018). Meanwhile, in MMPs, variation modelling method by the SoV theory has been the hotspot in recent two decades. Huang, Shi, and Yuan (2003) and Djurdjanovic and Ni (2003) proposed an approximately linearised but implicit state space model to express variation propagation for MMPs. Zhou, Huang, and Shi (2003) explored the vectorial deviation representation and proposed a generic linear state space model in terms of differential motion vector (DMV) to describe the SoV. This work deduced detailed

---

mathematical expressions of datum-induced variation and fixture-induced variation, and it was known as the conventional SoV model. Subsequently, this model was further expanded in fixture layouts (Loose, Zhou, and Ceglarek 2007; Abellan-Nebot and Liu 2013; Yang, Jin, and Li 2017b), application objects (Du, Yao, and Huang 2015; Du et al. 2015; Wang, Du, and Xi 2020), and geometric dimensioning and tolerancing (GD&T) integration (Loose et al. 2010; Wang et al. 2017). Abellan-Nebot et al. (2012) modelled the spindle-thermal variations and the cutting-tool wear-induced variations during machining, and this model was called the extended SoV model. Detailed descriptions of existing research work on variation propagation modelling and applications were provided in a monograph (Shi 2006) and several reviews (Shi and Zhou 2009; Yang, Jin, and Li 2017a; Rezaei-Malek et al. 2019b). In summary, the researching trend of variation propagation modelling presents the following rules: from assembling to machining, from fuzzy system description to explicit representation of variation sources, and the applicable workpieces have become diversified, from simple box workpieces to more complex parts.

Common workpieces can be divided into three categories according to the structural stiffness: rigid, flexible and variable stiffness (Li et al. 2019). The stiffness of rigid workpiece is uniform and high such as solid casting without cavities, whereas that of flexible workpiece such as sheet is relatively low. With the diversification of product functional requirements, workpiece structure has been increasingly complex, and the stiffness may span a wide range in a single workpiece. For instance, a four-cylinder engine block as shown in Figure 1 is a typical variable stiffness structure (VSS) workpiece (Shao et al. 2018; Shao et al. 2019). One of the most conspicuous features is that it contains several closely spaced cylinders causing prominent and continuous change in wall thickness, which decide both the flexural and compressive stiffness in the case of material isotropic (Li et al. 2019). The flexural stiffness of this engine block varies from 3473 to 1,288,390 NâĹŹm^2 as the wall thickness varies from 13.5 to 97 mm (Du, Liu, and Xi 2015; Shao et al. 2018).

Compared to the rigid body, the overall stiffness of VSS workpiece is low and non-uniform due to the characteristics of multiple holes and local thin walls, which means when force is applied to the surface of workpiece, the thrust face will generate a larger deformation. Therefore, reflected in machining process, the locating datum feature will also generate more remarkable elastic deformation under the external force such as clamping force and cutting force, introducing additional variations into MMPs.

Figure 2 takes a simplified four-cylinder engine block machining as an example to indicate the effect of these variations on a VSS workpiece. Under the action of clamping force and cutting force, both the contact points on datum surface and locators are elastically deformed, and these variations will transmit to KPCs in the form of datum-induced variations and fixture-induced variations respectively. In addition, the magnitude of deformation differs when the force exerts on the surface of different structure regions. For example, the structure corresponding to locator 1 or 3 has a lower stiffness for the existence of cylinder hole, so that the deformation of contact point on datum surface is relatively large. Therefore, the non-uniform elastic deformation caused by external force during machining has a great influence on the final surface quality for a VSS workpiece.

However, variation propagation research in MMPs based on state space model all assumes that the workpiece is a rigid body and omit the elastic deformation in the features, not to mention the impact of workpiece stiffness change on the magnitude of elastic deformation. Consequently, existing SoV models cannot be readily applied to address the intrinsic
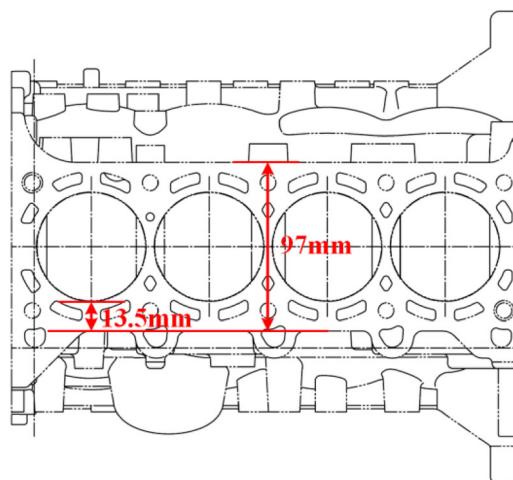

Figure 1.　The top view of a typical VSS workpiece.

(a) Elastic deformation variations on VSS workpiece   (b) The effect of variable stiffness structure
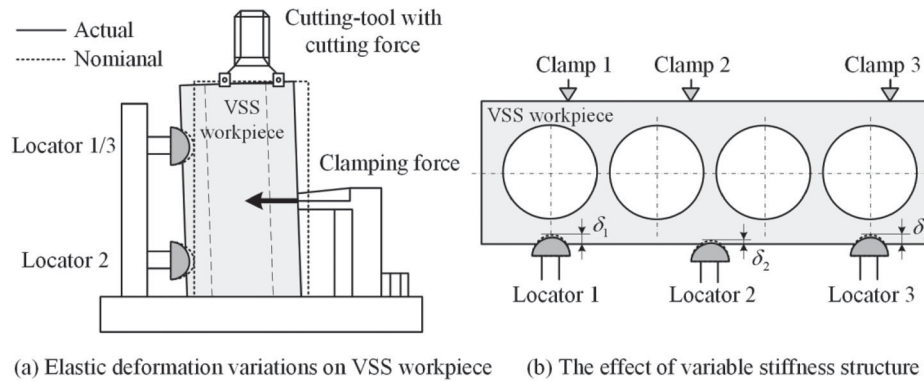
Figure 2. Example of elastic deformation variations on VSS workpieces

variation induction and propagation for VSS workpieces. It is necessary to consider the elastic deformation of variable stiffness structure, so that the SoV models can have better accuracy when facing such workpieces.

Methods available for elastic deformation analysis can be generally divided into numerical methods and analytic methods (Vasundara and Padmanaban 2014). Numerical method represented by finite element analysis (FEA) has been extensively applied for its superior applicability and operability, especially in the deformation analysis of complex VSS workpieces. However, if deformation analysis by FEA is adopted to state space modelling of variation propagation in MMPs, repeated iterations of multistage processes are hard to perform under huge computationally requirements (Yi et al. 2015). The lack of physical insights (Yi, Cheng, and Xu 2016) will also lead to difficulties in the intrinsic mapping relationship study from KCCs to KPCs, which will finally limit the further application of SoV model to process capability controlling and variation source diagnosis. Analytic method represented by elastic mechanics or contact mechanics can provide the analytic expression of displacement field on deformation point quickly and accurately, which overcomes the shortcomings of numerical method. However, most of the published analytic methods are limited to rigid or flexible workpiece, and little research has been done on VSS workpiece due to its complex structure. Recently, Li et al. (2019) proposed an analytic approach based on elastic mechanics to optimise the fixturing schemes of VSS workpieces. The idea of region division is meaningful for the deformation analysis of variable stiffness structure.

In this paper, a framework of variation propagation in MMPs for VSS workpieces is proposed to explicitly model the induction and propagation of elastic deformation variations caused by external force during machining. The elastic deformation variations on VSS workpieces are innovatively incorporated into the variation propagation model by analytic methods, which solves the limitation that the current SoV models can only deal with rigid workpieces without considering the stiffness change. That is the main contribution of this paper. Specifically, a cutting force model is developed to obtain the force distribution. Then, in view of the characteristics of VSS workpieces, region division is adopted and the analytic solutions of elastic deformation in different regions are solved by contact theory and elastic theory. Finally, the elastic deformation variations are incorporated into the variation propagation model. The proposed model will furnish quality improvement practitioners with a more comprehensive tool for accurate process evaluation, and thus, more effective monitoring and diagnosis for MMPs. The remainder of the paper is organised as follows. Section 2 shows the framework of the state space model of variation propagation in MMPs for VSS workpieces. In Sections 3 and 4, the solution of force distribution and elastic deformation are derived respectively. Section 5 presents the experimental validation results for this model. Concluding remarks and potential model applications are discussed in Section 6.

2. The proposed state space model

2.1. *Random deviation representation*

The model considers machining-, fixture- and datum-induced variations, including the elastic deformation variations in the machining process of VSS workpieces. These variations are introduced by and transmitted among key elements of manufacturing system, such as fixture locators, workpiece datum features, machined features, cutting-tool, machine-tool spindle, etc. Describing the stream of variations is equivalent to representing the propagation and conversion of those variations among key elements.

2.1.1. Coordinate system definition

Coordinate systems (CSs) involved in the model are defined to represent the variations of key elements (The notion with left superscript '0' means the nominal condition):

(1) Design coordinate system (DCS) is the reference for workpiece features during design. This CS will not deviate and it is generally defined at an accessible corner.
(2) Reference coordinate system (RCS) defines the reference for the position and orientation of all workpiece features at a specific stage, and it is generally defined the same as the local CS of the primary datum feature for simplification.
(3) Fixture coordinate system (FCS) defines the position and orientation of fixture according to the fixture layout, and it determines the position of each locator.
(4) Local coordinate system (LCS) is associated with one specific feature on workpiece, and it represents machined feature's position and orientation.
(5) Machine-tool component coordinate system (MCCS) is the CS collection of machine-tool (MCS), axes (ACS), spindle (SCS), cutting-tool (CCS) and cutting-tool tip (TPCS), which defines the position and orientation of each component of the machine-tool. The specific definition can refer to Abellan-Nebot et al. (2012).

These defined CSs can establish a generic framework for expressing the variations induction and propagation from TPCS to DCS along a chain. The chain consists of two sub-chains. The first sub-chain (from MCS to TPCS) has been well studied by Abellan-Nebot et al. (2012) which represents the impact of machining-induced variations including thermal spindle expansions and cutting-tool wear. The second sub-chain (from MCS to DCS) represents the effects of fixture- and datum-induced variations, including the elastic deformation variations for VSS workpieces which have not been studied.

2.1.2. Variation representation

To better define DMV for variation propagation, two CSs are constructed to express the location and variation relation. The position and the orientation of CS_A w.r.t. CS_B are defined by $\mathbf{r}_A^B = \left[(\mathbf{t}_A^B)^T \quad (\boldsymbol{\omega}_A^B)^T \right]^T$ which consists of a translation vector $\mathbf{t}_A^B = \begin{bmatrix} x_A^B & y_A^B & z_A^B \end{bmatrix}^T$ and a rotation vector $\boldsymbol{\omega}_A^B = \begin{bmatrix} \alpha_A^B & \beta_A^B & \gamma_A^B \end{bmatrix}^T$. The projections of CS_A coordinate origin on the three coordinates of CS_B are x_A^B, y_A^B, z_A^B and the orientation of CS_A coordinate axes can be obtained by sequentially rotating CS_B around z, y and z axes with Euler angles $\alpha_A^B, \beta_A^B, \gamma_A^B$ respectively.

The random deviation of a feature can be represented by DMV of its own CS w.r.t. another CS (Paul 1981). If CS_A is LCS_i and CS_B is RCS, the position and orientation of a specific feature w.r.t. the reference is $\mathbf{r}_A^B$, and the corresponding random deviation is defined by a DMV $\mathbf{x}_A^B = \left[(\mathbf{d}_A^B)^T \quad (\boldsymbol{\theta}_A^B)^T \right]^T$, where $\mathbf{d}_A^B = \Delta \mathbf{t}_A^B = \begin{bmatrix} \Delta x_A^B & \Delta y_A^B & \Delta z_A^B \end{bmatrix}^T$ contains three small translation deviations and $\boldsymbol{\theta}_A^B = \Delta \boldsymbol{\omega}_A^B = \begin{bmatrix} \Delta \alpha_A^B & \Delta \beta_A^B & \Delta \gamma_A^B \end{bmatrix}^T$ contains three small rotation deviations.

The DMV representation of random deviations is the basis for variation propagation modelling and DMVs can be transmitted by the following corollary to model the propagation and accumulation of deviations along the CSs chain (Zhou, Huang, and Shi 2003):

Corollary: Consider feature 1, 2 and RCS as shown in Figure 3. Feature 1 and 2 deviate from their nominal positions and orientations. Denoting $\mathbf{x}_1^R$ as the deviation of CS_1 w.r.t. RCS, $\mathbf{x}_2^R$ as the deviation of CS_2 w.r.t. RCS, and $\mathbf{x}_2^1$ as the deviation of CS_2 w.r.t. CS_1, the relationships among $\mathbf{x}_1^R, \mathbf{x}_2^R$ and $\mathbf{x}_2^1$ can be described by

$$\mathbf{x}_2^R = \begin{pmatrix} ({}^0\mathbf{R}_2^1)^T & -({}^0\mathbf{R}_2^1)^T \cdot ({}^0\hat{\mathbf{t}}_2^1) & \mathbf{I}_{3\times3} & \mathbf{0}_{3\times3} \\ \mathbf{0}_{3\times3} & ({}^0\mathbf{R}_2^1)^T & \mathbf{0}_{3\times3} & \mathbf{I}_{3\times3} \end{pmatrix} \cdot \begin{pmatrix} \mathbf{x}_1^R \\ \mathbf{x}_2^1 \end{pmatrix} = \mathbf{Q}_2^1 \cdot \mathbf{x}_1^R + \mathbf{x}_2^1 \tag{1}$$
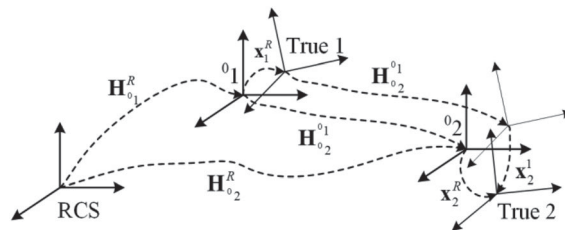

Figure 3. Transition of DMV when 1 and 2 deviate.

$$\mathbf{x}_2^1 = \begin{pmatrix} -({}^0\mathbf{R}_2^1)^T & ({}^0\mathbf{R}_2^1)^T \cdot ({}^0\hat{\mathbf{t}}_2^1) & \mathbf{I}_{3\times3} & \mathbf{0}_{3\times3} \\ \mathbf{0}_{3\times3} & -({}^0\mathbf{R}_2^1)^T & \mathbf{0}_{3\times3} & \mathbf{I}_{3\times3} \end{pmatrix} \cdot \begin{pmatrix} \mathbf{x}_1^R \\ \mathbf{x}_2^R \end{pmatrix} = -\mathbf{Q}_2^1 \cdot \mathbf{x}_1^R + \mathbf{x}_2^R \tag{2}$$

where ${}^0\mathbf{R}_2^1$ is the rotation matrix of ${}^0CS_2$ w.r.t. ${}^0CS_1$, and ${}^0\hat{\mathbf{t}}_2^1$ is the skew symmetric matrix associated with the translation vector ${}^0\mathbf{t}_2^1$.

Assuming that there are M features on a workpiece and the deviation of the nth feature w.r.t. RCS at stage k is a DMV $\mathbf{x}_{k,n}^{\text{RCS}}$ ($n = 1, 2, \ldots, M$), the state vector $\mathbf{x}(k) = \left[(\mathbf{x}_{k,1}^{\text{RCS}})^T \quad (\mathbf{x}_{k,2}^{\text{RCS}})^T \quad \cdots \quad (\mathbf{x}_{k,M}^{\text{RCS}})^T \right]^T$ is a stack of DMVs that represents the deviations that have been generated on a workpiece after k stage.

2.2. Framework for incorporating elastic deformation variations

Based on the vectorial deviation representation by DMVs, variation propagation in an N-stage MMP can be described by the state space model (Zhou, Huang, and Shi 2003):

$$\mathbf{x}(k) = \mathbf{A}(k-1) \cdot \mathbf{x}(k-1) + \mathbf{B}(k) \cdot \mathbf{u}(k) + \mathbf{w}(k) \tag{3}$$

$$\mathbf{y}(k) = \mathbf{C}(k) \cdot \mathbf{x}(k) + \mathbf{v}(k) \tag{4}$$

where $\mathbf{A}(k-1) \cdot \mathbf{x}(k-1)$ represents the deviations transmitted by the datum features introduced from previous stages; $\mathbf{B}(k) \cdot \mathbf{u}(k)$ represents the deviations induced at current stage due to fixture-induced variations and machining-induced variations; $\mathbf{C}(k) \cdot \mathbf{x}(k)$ represents the deviations of KPCs in the measurement; $\mathbf{w}(k)$ and $\mathbf{v}(k)$ define the un-modelled system errors and the measurement noise respectively. The coefficient matrices $\mathbf{A}(k-1)$, $\mathbf{B}(k)$ and $\mathbf{C}(k)$ are determined by product and process information.

The process variations at stage k are denoted as $\mathbf{u}(k) = \left[(\mathbf{u}_f^k)^T \quad (\mathbf{u}_m^k)^T \right]^T$, where $\mathbf{u}_f^k = [\Delta l_1^k \ \Delta l_2^k \ \Delta l_3^k \ \Delta l_4^k \ \Delta l_5^k \ \Delta l_6^k]^T$ is the wear deviation of fixture locators and $\mathbf{u}_m^k$ is the machining-induced variations that models the overall deviation of the first sub-chain, i.e. $\mathbf{x}_{\text{TPCS}}^{\text{MCS}}$. $\mathbf{u}_m^k$ has been well built with the consideration of spindle-thermal variations and cutting-tool wear variations (Abellan-Nebot et al. 2012) while the modelling of $\mathbf{x}(k-1)$ and $\mathbf{u}_f^k$ in Equation (3) for VSS workpieces
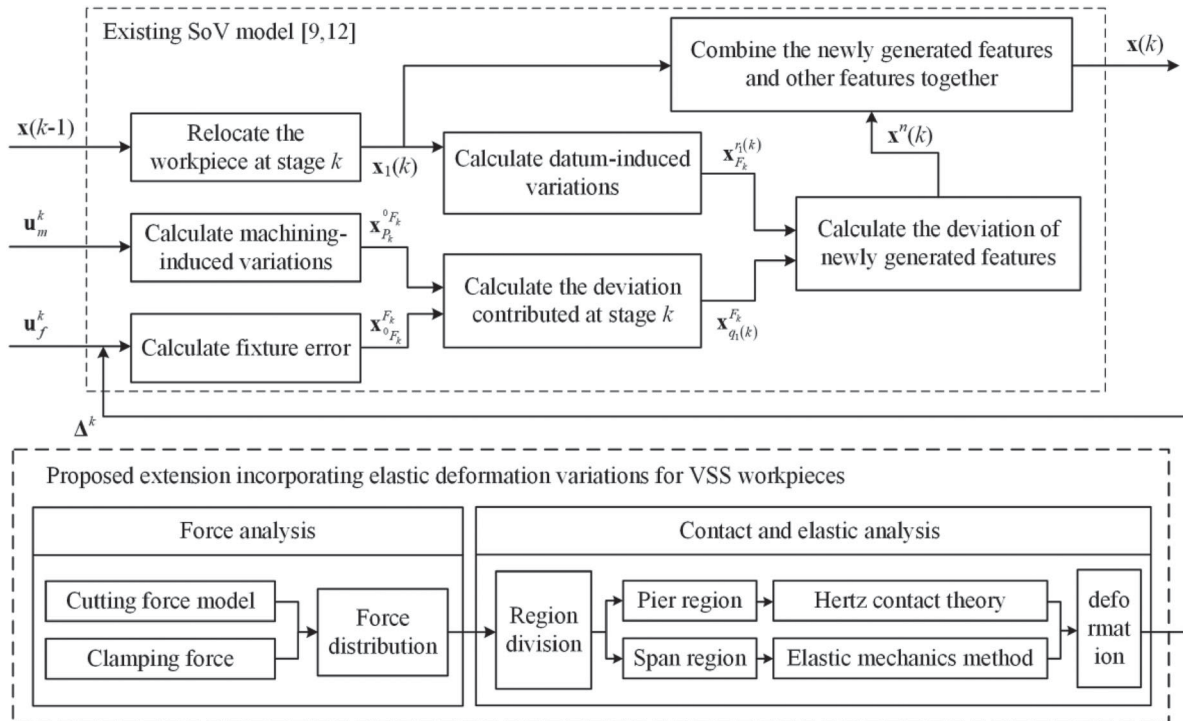

Figure 4. Summary of the procedure to derive the extended state space model.

is imperfect due to the omission of elastic deformation on datum features and locators. For workpiece datum feature, the elastic deformation is generated during the machining process at stage k, and these variations are only limited to the contact areas with locators, so it is difficult to express the elastic deformation variations on datum feature by linear DMV $\mathbf{x}(k-1)$. Therefore, in this paper, the deformation of datum feature and locator is integrated at the contact point as Δ_i^k and the stack of integrated deformation $\mathbf{\Delta}^k = [\Delta_1^k \ \Delta_2^k \ \Delta_3^k \ \Delta_4^k \ \Delta_5^k \ \Delta_6^k]$ is added as a new part to the wear deviation of fixture locators, i.e. $\mathbf{u}(k) = \left[(\mathbf{u}_f^k + \mathbf{\Delta}^k)^T \ (\mathbf{u}_m^k)^T \right]^T$ for the extended framework of variation propagation in MMPs for VSS workpieces. In this way, the elastic deformation of datum contact points and locators can be fully considered, and these variations are only embodied and controlled in state space model by the form of fixture-induced variations, eliminating the need to study complex nonlinear form error.

The framework of the proposed method is shown in Figure 4, and the main steps are described as follows.

- Step 1: Develop an exponential instantaneous cutting force model of the face milling process to obtain the cutting force during machining. Combine the clamping force and the equilibrium condition to obtain the force distribution at the contact points for maintaining the stability of the manufacturing system.
- Step 2: Analyse the elastic deformation on contact stress points for VSS workpiece machining. A division strategy is implemented to divide the VSS elastomer into two types of characteristic regions denoted by pier and span. The analytic solutions of deformation field in different regions are derived using contact mechanics and elastic mechanics.
- Step 3: Superimpose total deformation $\mathbf{\Delta}^k$ on the wear deviation of fixture locator, incorporating the elastic deformation variations into state space modelling of variation propagation in MMPs for VSS workpieces.

3. Force analysis

Locating and clamping is to keep the workpiece stable in desired position and orientation during the machining process (Abellan-Nebot et al. 2012). The objective of this section is to obtain the force distribution at the contact points between locators and datum feature when the workpiece maintains static equilibrium under the action of cutting force and clamping force during the machining process.

3.1. Exponential instantaneous cutting force model

For an N-tooth face milling cutter as shown in Figure 5(a), the cutting edge of each tooth is divided into M micro elements. $dF_{j,l}$ is the cutting force of the lth micro element on the cutting edge of jth tooth, where $l = 1, 2, \ldots, M$ and $j = 1, 2, \ldots, N$. It is determined by the cutting-tool/workpiece material, instantaneous cutting thickness and micro element's height, and it can be decomposed to tangential force dF_t, radial force dF_r and axial force dF_a as shown in Figure 5(b). Transforming to
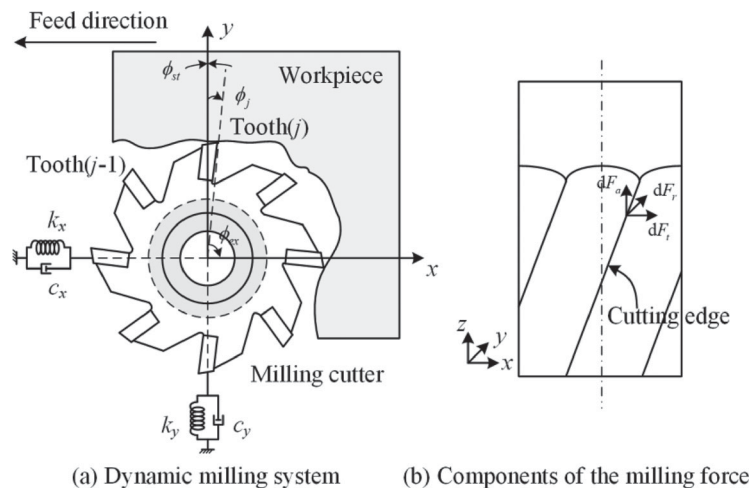

(a) Dynamic milling system   (b) Components of the milling force

Figure 5. Cutting force modelling for milling process.

MCS, the cutting force components of $dF_{j,l}$ along x, y, and z axes can be represented as

$$\begin{cases} dF_x = K_{tc}h dz + K_{te}dz = -dF_{t,j,l}\cos\phi_{j,l} - dF_{r,j,l}\sin\phi_{j,l} \\ dF_y = K_{rc}h dz + K_{re}dz = dF_{t,j,l}\sin\phi_{j,l} - dF_{r,j,l}\cos\phi_{j,l} \\ dF_z = K_{ac}h dz + K_{ae}dz = dF_{a,j,l} \end{cases} \tag{5}$$

where K_{tc}, K_{rc}, K_{ac}, K_{te}, K_{re} and K_{ae} are undetermined coefficients depending on the type of cutting force model; dz is the height of micro element; $h = f_z \sin\phi_{j,l}$ is the instantaneous cutting thickness, where f_z is the feed per tooth and $\phi_{j,l}$ is the radial immersion angle.

For the exponential instantaneous model (Hoon Ko and Cho 2005; Wan et al. 2009), the cutting force coefficients are given as follows: $K_{te} = K_{re} = K_{ae} = 0$, $K_{tc} = K_t h^{-p}$, $K_{rc} = K_r h^{-q}$, $K_{ac} = K_a h^{-r}$, where K_t, K_r and K_a denote the tangential, radial and axial force coefficients while p, q, r are the corresponding cutting thickness index. Consequently, for each round of the cutter, the average cutting force components along x, y, and z axes can be calculated by

$$\begin{cases} F_{A,x} = \dfrac{a_p N}{2\pi}K_r f_z^{1-q}\int_0^\pi (\sin\phi)^{2-q}d\phi \\ F_{A,y} = \dfrac{a_p N}{2\pi}K_t f_z^{1-p}\int_0^\pi (\sin\phi)^{2-p}d\phi \\ F_{A,z} = \dfrac{a_p N}{2\pi}K_a f_z^{1-r}\int_0^\pi (\sin\phi)^{1-r}d\phi \end{cases} \tag{6}$$

Dividing both sides of the Equation (6) by $a_p N$ and taking the logarithm, a linear expression with $\ln f_z$ as the independent variable can be derived as

$$\ln\left(\frac{F_{A,q}}{a_p N}\right) = B_q \ln f_z + A_q, \quad q = x, y, z \tag{7}$$

A_q and B_q can be fitted by the least square method (Wan et al. 2014) through a series of experimental tests of cutting force using different cutting parameters. Therefore, the formulas for calculating the cutting force coefficient are given as follows

$$\begin{cases} q = 1 - B_x, \ p = 1 - B_y, \ r = 1 - B_z \\ K_r = \dfrac{2\pi e^{A_x}}{\int_0^\pi (\sin\phi)^{1+B_x}d\phi}, \ K_t = \dfrac{2\pi e^{A_y}}{\int_0^\pi (\sin\phi)^{1+B_y}d\phi}, \ K_a = \dfrac{2\pi e^{A_z}}{\int_0^\pi (\sin\phi)^{B_z}d\phi} \end{cases} \tag{8}$$

3.2. Force distribution

Strategically placing locators and clamps around the workpiece and applying the clamping force with appropriate magnitude, fixture scheme can achieve accurate locating during machining. By regarding the fixture-workpiece as an integrated system, the static equilibrium conditions for stability are analysed to calculate the force distribution exerting on the contact points between the locators and the datum surfaces.

As shown in Figure 6, the clamping force in x direction is provided by the screw rod of a clamping chuck device. To maintain the static equilibrium of the fixture-workpiece system, the fixed clamping force F_C exerted by the chuck with three clamps should be much bigger than cutting force $F_{A,x}$, which means the combination of external force still exerts a force on the clamping surface. Therefore, the counterforce from locators is applied on the datum contact points, causing elastic deformation on datum feature and locators, which eventually leads to the location error.

Supposing that the coordinates of these three contact points are $(0, y_1, z_1)$, $(0, y_2, z_2)$ and $(0, y_3, z_3)$ w.r.t. CS_L respectively. According to the static equilibrium conditions, the force distribution in each contact point i.e. F_{L1}, F_{L2} and F_{L3} can be obtained by the following equation set.

$$\begin{cases} F_C - F_{A,x} = F_{L1} + F_{L2} + F_{L3} \\ F_{L1}\cdot|y_1| - F_{L2}\cdot|y_2| - F_{L3}\cdot|y_3| = 0 \\ F_{L1}\cdot|z_1| - F_{L2}\cdot|z_2| + F_{L3}\cdot|z_3| = 0 \end{cases} \tag{9}$$

Similarly, it is also possible to calculate the force distribution in the case of the direction has different numbers of locators. The force distribution will be the load input for following elastic analysis and contact analysis.
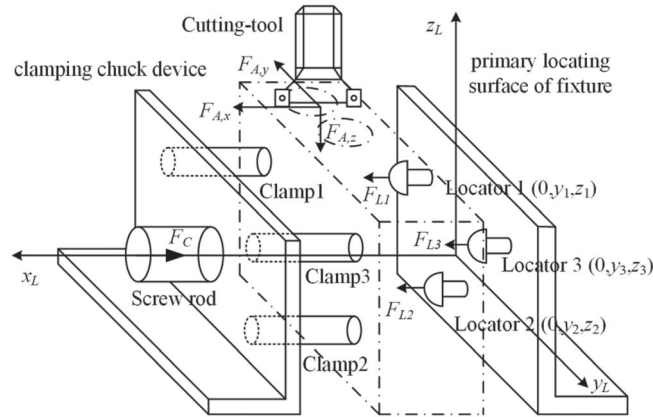
Figure 6. Force distribution of locators.

4. Elastic deformation analysis

The external force-induced deformation is hard to calculate directly due to the complex structure of VSS workpieces. In this section, a novel systematic method based on elastic mechanics and contact mechanics is derived for deformation analysis. The deformation analytic solutions of datum contact points and locators are given.

4.1. Region division

As illustrated in Figure 2, the magnitude of deformation is non-uniform when the force exerts on the surface of different structure regions due to the variable stiffness feature. Therefore, for VSS workpieces, it is practically impossible to analytically calculate the displacement fields for all contact points on datum surface by a universal formula. To address this issue, a region division strategy is proposed.

For a simplified four-cylinder engine block that retains the most important geometric feature, it is firstly divided into three regions by two parallel sections as shown in Figure 7, where a, b, H denote the length, width, height of the engine block respectively and R_b denotes the radius of the cylinder. Constrained by practical processing conditions, three pairs of locator-clamp are concentrated on the primary locating datum plane and its opposite plane, i.e. resultant of external force perpendicularly exerts on the flank of region 1 while the counterforce from three locators exerts to the flank of region 2. According to the characteristics of variable stiffness (Li et al. 2019), region 2 can be further divided into several sub-regions, including two types: pier region and span region. Since different sub-regions have different stiffness conditions, this region division strategy facilitates the calculation of non-uniform elastic deformation of corresponding sub-region separately.
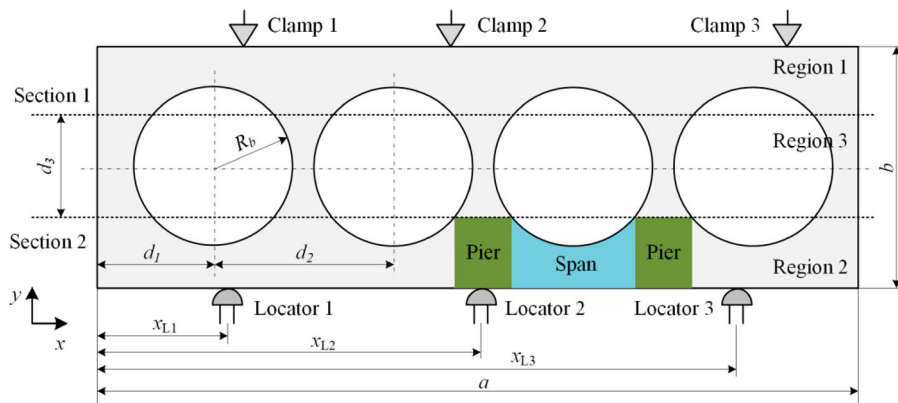

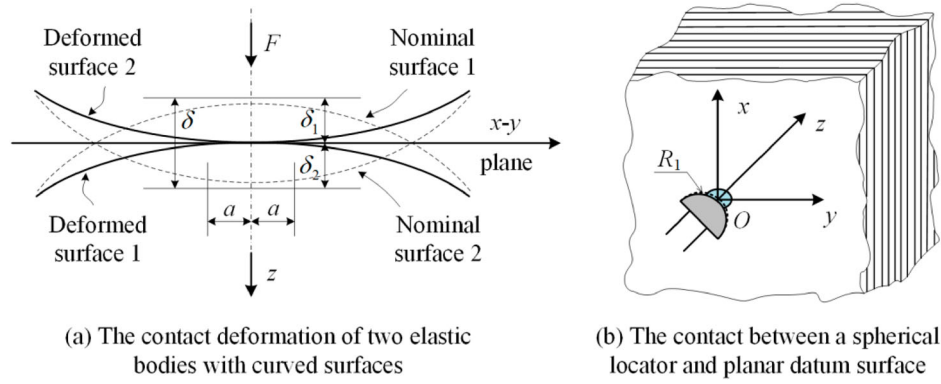Figure 7. Region division of a simplified four-cylinder engine block.

(a) The contact deformation of two elastic bodies with curved surfaces

(b) The contact between a spherical locator and planar datum surface

Figure 8. The contact of pier region.

4.2. Pier region deformation

The pier region has two major characteristics: the stiffness is relatively high and there is no need to consider the influence of variable stiffness. Without loss of generality, it is assumed that fixtures are based on spherical locators and datum surfaces are planar.

Considering the counterforce from locator is perpendicularly exerted on the flank of a pier region, this problem can be equivalent to the classic Boussinesq problem (Gao et al. 2013), i.e. elastic analysis of the semi-infinite space whose boundary is exerted with a vertical load. Hertz contact theory can be directly adopted to solve the total deformation of locator and datum feature.

As shown in Figure 8(a), according to Hertz contact theory (Yeh and Liou 1999), the total contact deformation δ for two elastic bodies with curved surfaces are as follows

$$\delta = \delta_1 + \delta_2 = \left(\frac{9}{16 \cdot R_* \cdot E_*{}^2} \right)^{1/3} \cdot F^{2/3} \tag{10}$$

where F is the total compression load which can be derived from force distribution in Section 3.2; R_* and E_* are the equivalent radius and the equivalent Young's modulus of two contact bodies respectively. These two parameters are defined by

$$\begin{cases} \dfrac{1}{R_*} = \dfrac{1}{R_1} + \dfrac{1}{R_2} \\ \dfrac{1}{E_*} = \dfrac{1 - \upsilon_1{}^2}{E_1} + \dfrac{1 - \upsilon_2{}^2}{E_2} \end{cases} \tag{11}$$

where R_1 and R_2, E_1 and E_2, υ_1 and υ_2 are the radii, Young's moduli and Poisson ratios of two contact bodies respectively. For the contact between a spherical locator and planar datum surface as shown in Figure 8(b), the radius of the plane is infinite, i.e. $R_2 \to \infty$, so that R_* is equal to the radius of locator R_1. The result of Equation (10) is the total deformation of locator and the datum feature, i.e. $\Delta_i^k = \delta$ when the locator i is contact with pier region. Note that for the contact between any other type of fixture locators and datum surfaces, Equation (10) can be modified accordingly (Yeh and Liou 1999).

4.3. Span region deformation

The main characteristic of span region is that the flexure stiffness is relatively low and it is not constant. Therefore, the span region can be deemed as an elastic plate with variable stiffness (Li et al. 2019). The compression load F is the input of the elastic analysis for span region. Since the flexural stiffness of locator is much larger than that of the workpiece when the force is applied to the span region, the elastic deformation of locator can be omitted. The analytic solution of datum surface deformation can be calculated by elastic mechanics method based on the double trigonometric series expansion.

Before the elastic analysis, three hypotheses and one lemma listed in Timoshenko and Goodier (1971) should be introduced, which are all commonly used in elastic mechanics. When F is perpendicularly loaded on the flank of a span region as shown in Figure 9(a), the basic equations of elastic analysis, including strain displacement equations and elastic constitutive equations are demonstrated as follows:
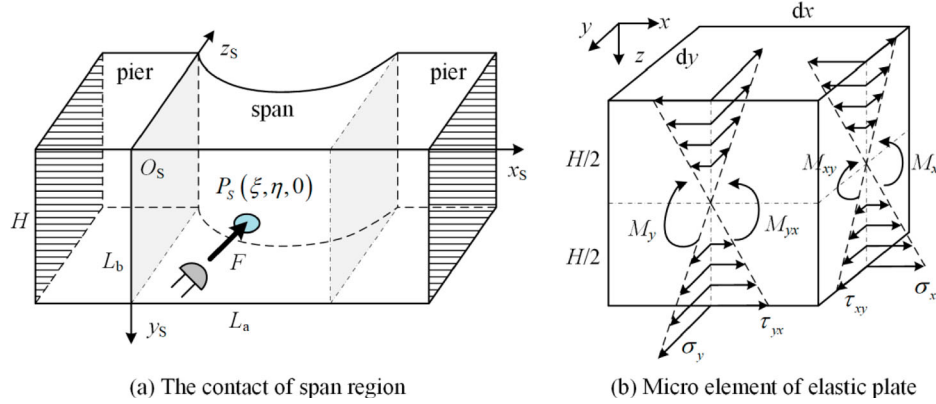
(a) The contact of span region   (b) Micro element of elastic plate

Figure 9. The elastic deformation analysis of span region.

The strain displacement equations are given as

$$
\begin{cases}
\varepsilon_x = \dfrac{\partial u}{\partial x} = -z\dfrac{\partial^2 w}{\partial x^2} = z\kappa_x \\[2mm]
\varepsilon_y = \dfrac{\partial v}{\partial y} = -z\dfrac{\partial^2 w}{\partial y^2} = z\kappa_y \\[2mm]
\gamma_{xy} = \dfrac{\partial v}{\partial x} + \dfrac{\partial u}{\partial y} = -2z\dfrac{\partial^2 w}{\partial x \partial y} = 2z\kappa_{xy}
\end{cases}
\tag{12}
$$

where ε_x, ε_y and γ_{xy} denote the normal strain along the x-axis, y-axis and the shear strain respectively while κ_x, κ_y and κ_{xy} denote the curvatures along the x-axis, y-axis, and the twist rate respectively.

The elastic constitutive equations are given as

$$
\begin{cases}
\sigma_x = \dfrac{E}{1-v^2}(\varepsilon_x + v\varepsilon_y) \\[2mm]
\sigma_y = \dfrac{E}{1-v^2}(\varepsilon_y + v\varepsilon_x) \\[2mm]
\tau_{xy} = \dfrac{E}{2(1+v)}\gamma_{xy}
\end{cases}
\tag{13}
$$

where σ_x, σ_y and τ_{xy} denote the normal stress along the x-axis, y-axis and the shear stress respectively.

Substituting Equation (12) into (13), yields

$$
\begin{cases}
\sigma_x = -\dfrac{Ez}{1-v^2}\left(\dfrac{\partial^2 w}{\partial x^2} + v\dfrac{\partial^2 w}{\partial y^2}\right) = \dfrac{Ez}{1-v^2}(\kappa_x + v\kappa_y) \\[2mm]
\sigma_y = -\dfrac{Ez}{1-v^2}\left(\dfrac{\partial^2 w}{\partial y^2} + v\dfrac{\partial^2 w}{\partial x^2}\right) = \dfrac{Ez}{1-v^2}(\kappa_y + v\kappa_x) \\[2mm]
\tau_{xy} = -\dfrac{Ez}{1+v}\dfrac{\partial^2 w}{\partial x \partial y} = \dfrac{Ez}{1+v}\kappa_{xy}
\end{cases}
\tag{14}
$$

For obtaining the deflection equation and the boundary conditions of elastic analysis, an elastic micro element of elastic plate is shown in Figure 9(b), where dx, dy and h represent the length, width and height of the micro element respectively. The internal moment of this micro element is given by Timoshenko and Goodier (1971)

$$
\begin{cases}
M_x = \int_{-h/2}^{h/2} \sigma_x z\,dz = -D\left(\dfrac{\partial^2 w}{\partial x^2} + v\dfrac{\partial^2 w}{\partial y^2}\right) = D(\kappa_x + v\kappa_y) \\[2mm]
M_y = \int_{-h/2}^{h/2} \sigma_y z\,dz = -D\left(\dfrac{\partial^2 w}{\partial y^2} + v\dfrac{\partial^2 w}{\partial x^2}\right) = D(\kappa_y + v\kappa_x) \\[2mm]
M_{xy} = \int_{-h/2}^{h/2} \tau_{xy} z\,dz = -D(1-v)\dfrac{\partial^2 w}{\partial x \partial y} = D(1-v)\kappa_{xy}
\end{cases}
\tag{15}
$$

where D is the flexural stiffness and it can be defined as

$$D = \frac{E \cdot h^3}{12(1 - v^2)} \tag{16}$$

Denoting the external load function as $F(x, y)$, the deflection equation can be given as follows

$$\frac{\partial^4 w}{\partial x^4} + 2\frac{\partial^4 w}{\partial x^2 \partial y^2} + \frac{\partial^4 w}{\partial y^4} = \frac{F(x, y)}{D} \tag{17}$$

And the boundary conditions for a single span region can be derived as

$$\begin{cases} w = 0, \ \dfrac{\partial^2 w}{\partial x^2} = 0 \text{ for } x = 0 \text{ and } L_a \\ M_y = 0, \ M_{yx} = 0 \text{ for } y = 0 \text{ and } L_b \end{cases} \tag{18}$$

where $L_a = \sqrt{4R_b{}^2 - d_3{}^2}$, $L_b = H$ are the length and width of the flank of span region and both are constants which can be obtained directly from Figure 7.

Under the given boundary conditions, the double trigonometric series expansion (Tang and Liu 2008; Zhang et al. 2016) is applied to the external load $F(x, y)$ and the deflection $w(x, y)$ as Equations (19) and (20), so that the analytic solution to the deflection can be eventually obtained in the form of a function of the given load based on the properties of the double trigonometric series.

$$F(x, y) = \sum_{m=1}^{\infty} \sum_{n=1}^{\infty} A_{mn} \sin\frac{m\pi x}{L_a} \sin\frac{n\pi y}{L_b} \tag{19}$$

$$w(x, y) = \sum_{m=1}^{\infty} \sum_{n=1}^{\infty} B_{mn} \sin\frac{m\pi x}{L_a} \sin\frac{n\pi y}{L_b} \tag{20}$$

where A_{mn} and B_{mn} are two coefficients listed as follows and the detailed derivation can be found in the Appendix based on the orthogonality of trigonometric functions.

$$A_{mn} = \frac{4}{L_a L_b} \int_0^{L_b} \int_0^{L_a} F(x, y) \sin\frac{m\pi x}{L_a} \sin\frac{n\pi y}{L_b} \, \mathrm{d}x\mathrm{d}y \tag{21}$$

$$B_{mn} = \frac{A_{mn}}{\pi^4 D \cdot ((m^2/L_a^2) + (n^2/L_b^2))} = \frac{4 \int_0^{L_b} \int_0^{L_a} F(x, y) \sin(m\pi x/L_a) \sin(n\pi y/L_b)\mathrm{d}x\mathrm{d}y}{\pi^4 D \cdot L_a L_b \cdot ((m^2/L_a^2) + (n^2/L_b^2))} \tag{22}$$

Substituting Equation (22) into (20), the deflection $w(x, y)$ can be obtained as

$$w = \frac{4}{\pi^4 \cdot L_a L_b \cdot D} \cdot \sum_{m=1}^{\infty} \sum_{n=1}^{\infty} \frac{\int_0^{L_b} \int_0^{L_a} F(x, y) \sin(m\pi x/L_a) \sin(n\pi y/L_b)\mathrm{d}x\mathrm{d}y}{((m^2/L_a^2) + (n^2/L_b^2))} \sin\frac{m\pi x}{L_a} \sin\frac{n\pi y}{L_b} \tag{23}$$

Since the thickness of a span region $h(x)$ varies continuously along the x-axis direction, the flexural stiffness $D(x)$ can be derived based on Equation (16) as

$$D = \frac{E}{12(1 - v^2)} \cdot \left[\frac{b}{2} - \sqrt{R_b{}^2 - \left(\frac{L_a}{2} - x\right)^2} \right]^3 \tag{24}$$

Therefore, the result of Equation (23) is the deformation of datum feature, i.e. the deformation analytic solution is $\Delta_i^k = w$ when the locator i is contact with span region.
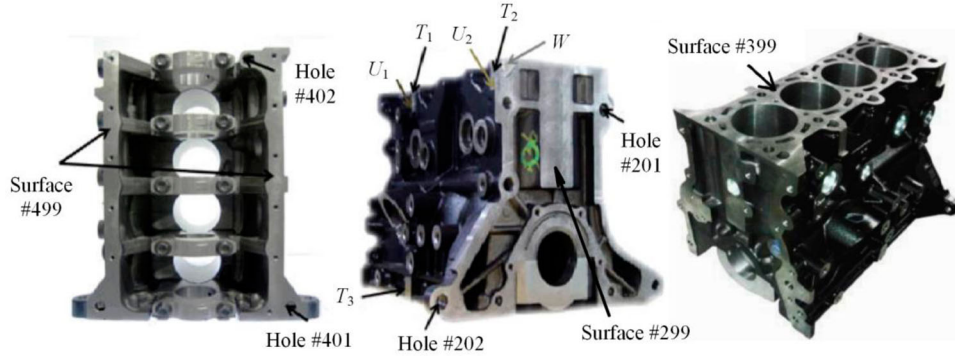
Figure 10. A four-cylinder engine block.

Table 1. Process description and nominal locations of key features.

Stage	Datum features	Process descriptions	${}^0\boldsymbol{\omega}_0^R$	${}^0\mathbf{t}_0^R$
OP10	$T_1, T_2, T_3, U_1, U_2, W$	Mill #299	$[0, 0, 0]$	$[-170.5, 138, 0]$
OP20	$T_1, T_2, T_3, U_1, U_2, W$	Semi-finish-mill #399	$[0, -\pi/2, \pi/2]$	$[-219, 248, -30.5]$
		Semi-finish-mill #499	$[0, \pi/2, \pi/2]$	$[18, 248, -30.5]$
OP30	$T_1, T_2, T_3, U_1, U_2, W$	Spot drill #401	$[\pi/2, 0, 0]$	$[18, 73, -312.5]$
		Spot drill #402	$[0, 0, \pi/2]$	$[18, 27, -17]$
OP40	#499, #401, #402	Spot drill #201	$[-\pi/2, 0, 0]$	$[-176.5, 201, 0]$
		Spot drill #202	$[0, \pi/2, 0]$	$[0, 0, 0]$
OP50	#299, #201, #202	Finish-mill #499	$[0, \pi/2, \pi/2]$	$[17.5, 248, -30.5]$
OP60	#499, #401, #402	Finish-mill #399	$[0, -\pi/2, \pi/2]$	$[-218.5, 248, -30.5]$

5. Case study

To verify the proposed variation propagation model for VSS workpieces, a six-stage machining process of the four-cylinder engine block (see Figure 10) is applied in this case.

The process is implemented by a DMG-HSC-75 computer numerical control (CNC) machining centre. Table 1 describes the six stages, illustrates the datum features in each stage and the nominal locations of key features w.r.t. RCS. Specifically, first two stages are milling processes, followed by spot drilling hole #401 and #402. T_1, T_2, T_3, U_1, U_2 and W are rough datum features for OP10 to OP30. The deviation of #499 machined at OP20 and the deviations of two holes drilled at OP30 are important variation sources for the machining features at OP40 and OP60. Similarly, the datum-induced errors from OP10 and OP40 accumulate deviations at OP50, which construct the stream of variation. After OP60, the machined workpiece is moved to the inspection stage to measure two KPCs defined by the surface #399 and #499.

Considering the locating and clamping scheme of each stage, the primary datum feature of OP10 to OP30 (T_1, T_2 and T_3) is on the flank of the engine block, and that of OP50 is the end face #299. In these four stages, due to the existence of the cylinder, the stiffness of the workpiece in primary locating direction is relatively low and the stiffness change is significant, which will bring additional elastic deformation variations to MMP under the action of cutting force and clamping force. These variations are difficult to introduce and propagate in the previous SoV models.

In this section, the cutting force coefficients are firstly solved by least squares fitting based on a series of experiments, and the calculated cutting force is combined with the clamping force to obtain the force distribution at the contact points, which is the input of following elastic deformation analysis. In the verification step, two KPCs' deviations obtained by the proposed method are compared to real machining process and existing SoV methods to prove the validity and accuracy of the new model. The predefined parameters in this case are listed in Table 2.

5.1. Elastic deformation variations

5.1.1. Cutting force coefficient experiments

In order to obtain the coefficients A_q and B_q of the exponential instantaneous cutting force model, nine groups of experiments are implemented to measure the cutting force for univariate linear regression of Equation (7). The experiments are performed on a quarter of engine block by DMG-HSC-75 CNC machining centre, and Table 3 gives the experiment parameters in

Table 2. Predefined parameters.

Description (symbol)	Value
length of the engine block (a)	326.5 mm
width of the engine block (b)	108 mm
height of the engine block (H)	236 mm
radius of the cylinder (R_b)	35 mm
radius of the locator (R_1)	5 mm
distance from the first centre line to the front face (d_1)	50 mm
distance between two adjacent centre line (d_2)	75.5 mm
distance between two sections (d_3)	30 mm
poisson ratio of locator (high carbon steel) (v_1)	0.25
poisson ratio of grey cast iron HT250 (v_2)	0.27
elastic modulus of locator (high carbon steel) (E_1)	200 GPa
elastic modulus of grey cast iron HT250 (E_2)	140 GPa

Table 3. Machining parameters for each group.

No.	N	a_p (mm)	f_z (mm)
1	6	0.1	0.1
2	8	0.15	0.12
3	10	0.2	0.14
4	8	0.12	0.16
5	10	0.17	0.18
6	6	0.22	0.2
7	10	0.08	0.22
8	6	0.12	0.24
9	8	0.18	0.26

detail. Since the machining parameter of V_s has no effect in Equation (7), it is preliminary fixed to 400 rpm in each group of experiment.

The raw cutting force signals are measured by 9027C Kistler three-component dynamometer. The signals are intercepted for 8 s in stable machining phase and processed by a 2-order low pass filter. The lower edge frequency of the filter is 50 Hz and the upper one is 100 Hz. The filtered cutting force signals are shown in Figure 11.

By calculating the average magnitude of cutting force along each coordinate axis under different groups of experiment parameter, the point estimation based least square method is applied to Equation (7) to estimate the coefficients of regression equation, i.e. undetermined coefficients of the cutting force model. The significance test of regression equation shows a significant linear correlation, so the results are reasonable. Table 4 shows the cutting force coefficients in all directions along the coordinate axis, which can be adopted to calculate the cutting force in primary locating direction and served as the input to the following elastic deformation analysis.

5.1.2. *Solution of elastic deformation*

Based on the cutting force and the predetermined clamping force, for the stages that need to consider elastic deformation variations, the force distributions at the contact points between locators and datum features can be calculated by the method of Section 3.2. For the first two stages, the force distribution is 101, 152 and 130 N at three contact points in primary locating direction, of which L_1 and L_3 correspond to the span region and L_2 corresponds to the pier region. The magnitude of elastic deformation at L_1 and L_2 is calculated in detail in this section, and the deformation of L_3 and other stages, such as OP50, can be solved similarly to obtain the integrated deformation $\boldsymbol{\Delta}$.

(a) Deformation of the pier region corresponding to L_2

The force known as 152 N is perpendicularly exerted on the flank of a pier region as shown in Figure 8(b). The material of the engine block is the grey cast iron HT250 and that of the locator is high carbon steel. The necessary information of material is given in Table 2. The equivalent radius and the equivalent Young's modulus are

$$\begin{cases} R_* = R_1 = 5 \text{ mm} \\ E_* = \left(\frac{1-0.25^2}{2\times10^{11}} + \frac{1-0.27^2}{1.4\times10^{11}} \right)^{-1} = 88.42 \text{ GPa} \end{cases}$$
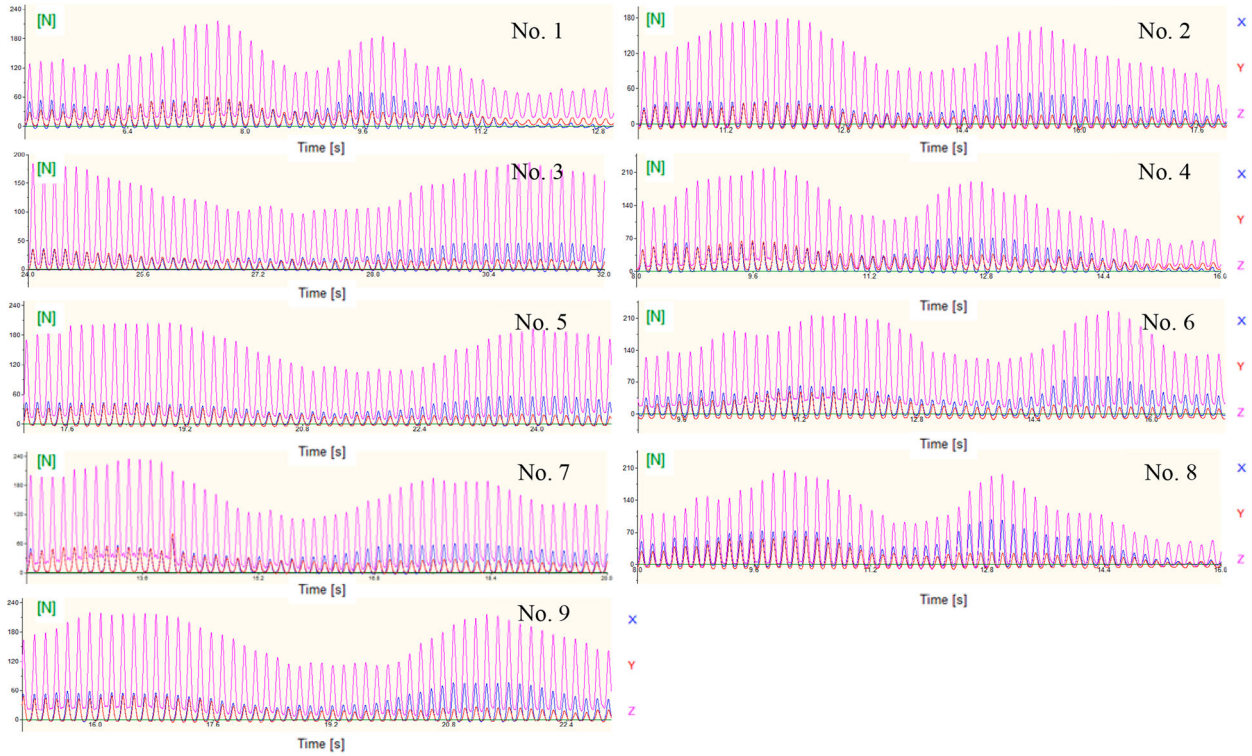
Figure 11.   The filtered cutting force signal of nine sets of experiments.

Table 4.   Undetermined coefficients of cutting force model.

Coefficient	A_x	A_y	A_z	B_x	B_y	B_z
Value	6.5408	6.8744	7.1703	0.2413	0.3341	0.5113

According to Equation (10), the total contact deformation δ is calculated as

$$\delta = \left(\frac{9}{16 \times 0.005 \times (88.42 \times 10^9)^2}\right)^{1/3} \cdot 152^{2/3} = 6.93 \times 10^{-6} \text{ m} = 0.00693 \text{ mm}$$

(b)   Deformation of the span region corresponding to L_1

The force known as 101 N is perpendicularly exerted on the flank of a span region as shown in Figure 9(a). The coordinate of the stress point is P_S (42, 31, 0) w.r.t. the local CS_S. According to Equation (23), the deformation w is calculated as

$$w = \frac{4 \times 12 \times 101(1 - 0.27^2)}{\pi^4 \times 64 \times 236 \times 1.4 \times 10^5 \times \left[54 - \sqrt{35^2 - (32-x)^2}\right]} \cdot \sum_{m=1}^{\infty}\sum_{n=1}^{\infty} \frac{\sin(42m\pi/64)\sin(31n\pi/236)}{((m^2/64^2) + (n^2/236^2))} \sin\frac{m\pi x}{64} \sin\frac{n\pi y}{236}$$

By MATLAB programming, the displacement field of datum surface is shown in Figure 12. When the iteration times exceed 12, the displacement field stays approximately the same, which demonstrates the fast convergence of the double trigonometric series method in solving elastic deformation of the span region. Although the force on span region is much smaller than that on pier region, the magnitude of deformation is more significant due to the characteristics of VSS workpiece. The maximum deformation at this contact point is 0.0207 mm, and its impact should not be ignored in MMPs.

(c)   Finite element simulation

To validate the magnitude of the elastic deformation calculated by proposed approach, a dynamic explicit FEA is adopted to simulate the machining process by the software of ABAQUS. In the mesh, there are 1,887,415 nodes and 4,264,337
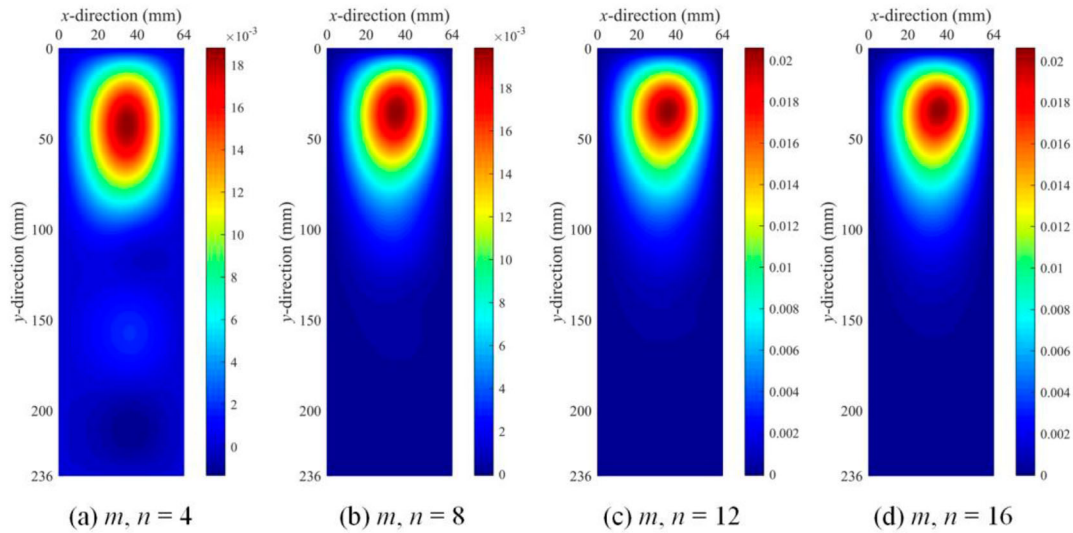
Figure 12. Deformation of a span region by double trigonometric series method.
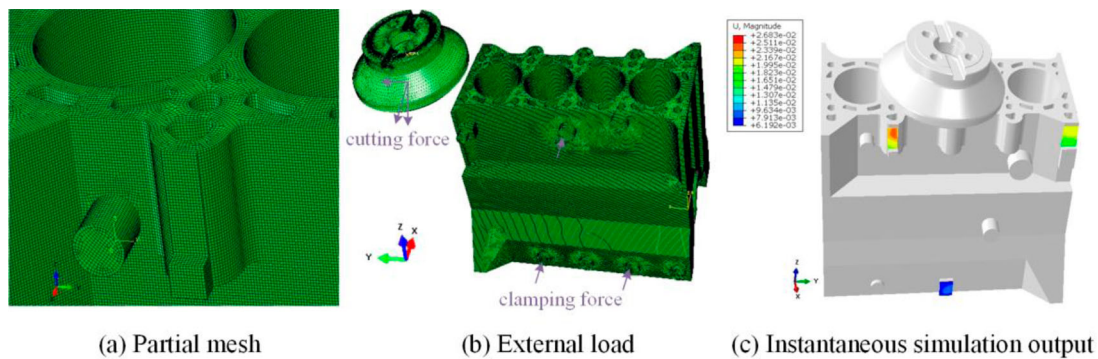

Figure 13. Dynamic explicit FEA simulation.

elements for discretization, and Figure 13(a) depicts part of the mesh. To ensure the convergence and accuracy of FEA simulation, 1,168,234 of the elements are linear hexahedral elements of type C3D8 to improve the quality of the mesh. In the load module of FEA, external forces from clamps and cutting tool are exerted as shown in Figure 13(b). The boundary conditions and all input parameters are the same as the real machining. The average elastic deformation of contact point in primary locating direction is the focus.

The visualisation simulation output at a certain time is shown in Figure 13(c). In the process, the average deformation of L_2 is 0.00716 mm and that of L_1 is 0.0225 mm. Compared with the results by analytic calculations respectively, small differences prove the accuracy of the proposed approach in elastic deformation solution.

5.2. Results and discussion

To validate the model, some significant variation sources were intentionally added to the engine block machining process at each stage. For example, the machining operations were conducted with a spindle temperature close to 25°C to define the spindle-thermal variations, and a worn cutting-tool was used with a flank wear of 0.01 mm to define the cutting-tool wear-induced variations. The fixture error of first three stages was equal to [0.018, 0, 0.023, 0.012, 0, 0] and that of last three stages was [0, 0, 0.019, 0, 0, 0]. The real machining process is shown in Figure 14.

Following the procedure illustrated in Section 2, a variation propagation model for this six-stage machining process can be obtained and it is programmed using MATLAB. All vectors and matrices can be calculated by corresponding equations. The dimensions of two KPCs are measured by coordinate measuring machine (CMM) after MMP, and the comparison between experimental results, conventional SoV model, extended SoV model, and the proposed model are presented in Table 5 and Figure 15.
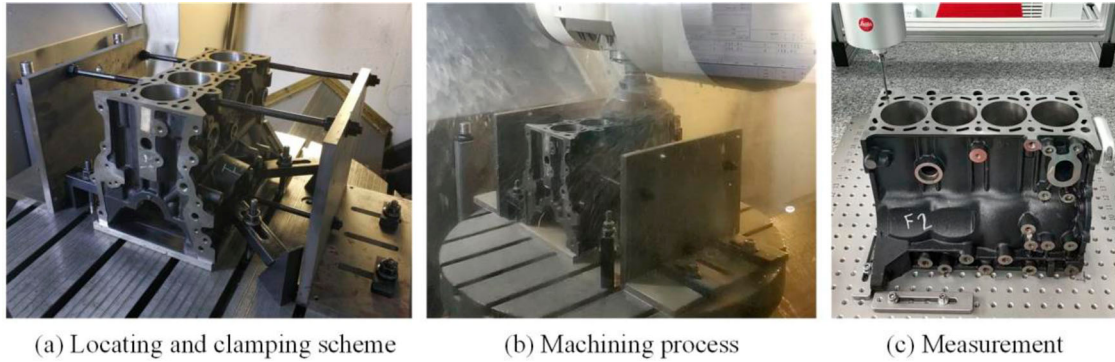
(a) Locating and clamping scheme   (b) Machining process   (c) Measurement

Figure 14. Real machining experiment.

Table 5. The results of measurement and model prediction.

Object		CMM	Conventional model		Extended model		Proposed model	
			Prediction	Error	Prediction	Error	Prediction	Error
z (mm)	#399	218.576	218.6232	0.0472	218.6084	0.0324	218.6037	0.0277
	#499	17.469	17.4746	0.0056	17.4728	0.0038	17.4719	0.0029

The superiority of the proposed model is discussed in two aspects: the comparison with real experiment results and the comparison with existing methods.

For the former one, the overall differences between the predicted values and actual measurements are reasonably small for both two KPCs, which illustrate the validity of the model. For example, the measurement result of surface #399 w.r.t. the origin of RCS is 218.576 mm, compared to 218.6037 mm predicted by the proposed model. The prediction error of 0.0277 mm is very small relative to the measured value. Another KPC of surface #499 presents the similar situation. The
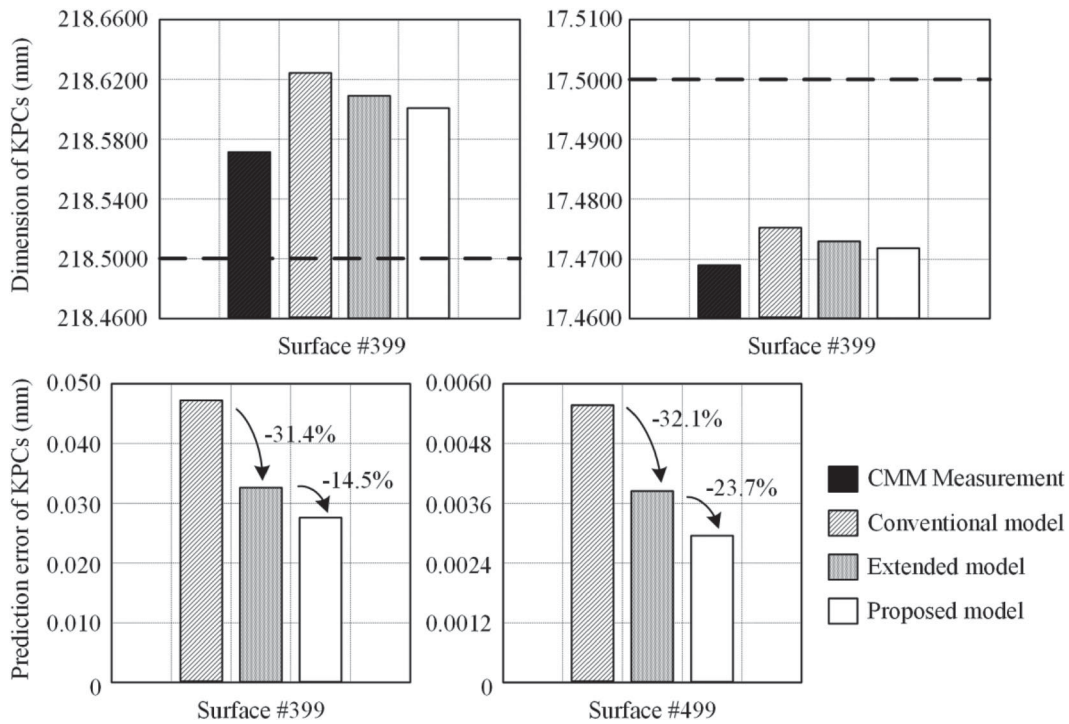

Figure 15. Deviation results comparison.

main reason for this small discrepancy is accounted to the noises which are difficult to model, such as the influence of vibration on machining processes or measurements.

For the comparison of the proposed model and existing methods, the advantages can be reflected in high accuracy and applicability. The conventional SoV model can only focus on the modelling of fixture-induced variations and datum-induced variations, other error factors such as cutting-tool wear, spindle-thermal variations, and elastic deformation variations are all treated as stochastic noises, i.e. $\mathbf{w}(k)$ in Equation (3). Therefore, the prediction error of conventional SoV model is the highest when these variation sources are intentionally added to the MMP. The extended SoV model incorporates some important machining-induced variations, so that the prediction errors of the two KPCs are decreased by 31.4% and 32.1% respectively, indicating the progress of SoV modelling. However, due to the neglect of the elastic deformation variations in VSS workpiece machining, the prediction error is still relatively large, which means neither of these two representative methods can accurately deal with VSS workpieces. The proposed model focuses on the variable stiffness structure of the workpiece and effectively considers the elastic deformation variations on MMP for VSS workpieces. It further reduces the inaccurately modelled parts of $\mathbf{w}(k)$, which means the prediction variance can be significantly smaller than that of previous methods. The accuracy on these two KPCs is increased by 14.5% and 23.7% respectively compared to extended SoV model, which means an average prediction improvement of 44.76% with respect to the conventional model when the machining object is a VSS workpiece and the elastic deformation variations are incorporated.

6. Conclusion

In spite of the success of SoV methods for variation propagation modelling in MMPs, the absence of elastic deformation variations may be an important factor to limit the use of this methodology. In this paper, a generic framework for incorporating the elastic deformation variations into the existing SoV models is proposed. This framework explicitly models the induction and propagation of elastic deformation variations during machining, and solves the limitation that the current SoV models can only handle rigid workpieces without considering the stiffness change. In view of the characteristics of VSS workpieces, region division is adopted and the analytic solutions of elastic deformation in different regions are solved by contact theory and elastic theory. The MMP of a four-cylinder engine block is presented in the case study, the prediction errors from the proposed model are notably lower than those from the existing SoV models, confirming the potential use of this model for VSS workpieces. Except for the engine block, with the diversification of products, this model can be applied to the production of more common workpieces as well, which only needs to be appropriately divided into regions based on the characteristics of the workpiece and solved by regions.

The current research of variation propagation is limited to the dimension error. Multi-scale variations including geometric error, waviness and roughness also participate in the variation propagation and accumulation, which lead to the overall deviations of machining feature. The study on the impacts of multi-scale variations to MMPs will be further investigated in future work. Furthermore, the proposed SoV model can be applied: (i) to optimise the layout of the fixture locators, and (ii) to some new applications for quality control of MMPs. For the first point, the placement of the fixture locators will have a great influence on the magnitude of elastic deformation during the VSS workpiece machining. By minimising the final deviations of KPCs, the optimal fixture layout can be obtained from the candidates by the optimisation algorithm. For the second point, the applications of this model will have great engineering values for VSS workpieces, such as process control and improvement, process-oriented tolerancing, and fault diagnosis.

References

Abellan-Nebot, José V., and Jian Liu. 2013. "Variation Propagation Modelling for Multi-Station Machining Processes with Fixtures Based on Locating Surfaces." *International Journal of Production Research* 51 (15): 4667–4681.

Abellan-Nebot, José V., Jian Liu, Fernando Romero Subirón, and Jianjun Shi. 2012. "State Space Modeling of Variation Propagation in Multistation Machining Processes Considering Machining-Induced Variations." *Journal of Manufacturing Science and Engineering* 134 (2): 021002.

Arizono, Ikuo, Kazunori Yoshimoto, and Ryosuke Tomohiro. 2020. "Variable Stage-Independent Double Sampling Plan with Screening for Acceptance Quality Loss Limit Inspection Scheme." *International Journal of Production Research* 58 (8): 2550–2559.

Behnamian, J., S. M. T. Fatemi Ghomi, B. Karimi, and M. Fadaei Moludi. 2017. "A Markovian Approach for Multi-Level Multi-Product Multi-Period Capacitated Lot-Sizing Problem with Uncertainty in Levels." *International Journal of Production Research* 55 (18): 5330–5340.

Djurdjanovic, Dragan, and Jun Ni. 2003. "Dimensional Errors of Fixtures, Locating and Measurement Datum Features in the Stream of Variation Modeling in Machining." *Journal of Manufacturing Science and Engineering* 125 (4): 716–730.

Du, Shichang, Changping Liu, and Lifeng Xi. 2015. "A Selective Multiclass Support Vector Machine Ensemble Classifier for Engineering Surface Classification Using High Definition Metrology." *Journal of Manufacturing Science and Engineering* 137 (1): 011003.

Du, Shichang, Rui Xu, Delin Huang, and Xufeng Yao. 2015. "Markov Modeling and Analysis of Multi-Stage Manufacturing Systems with Remote Quality Information Feedback." *Computers & Industrial Engineering* 88: 13–25.

Du, Shichang, Xufeng Yao, and Delin Huang. 2015. "Engineering Model-Based Bayesian Monitoring of Ramp-Up Phase of Multistage Manufacturing Process." *International Journal of Production Research* 53 (15): 4594–4613.

Du, Shichang, Xufeng Yao, Delin Huang, and Meng Wang. 2015. "Three-Dimensional Variation Propagation Modeling for Multistage Turning Process of Rotary Workpieces." *Computers & Industrial Engineering* 82: 41–53.

Duan, Guijiang, and Yang Wang. 2013. "QCs-linkage Model Based Quality Characteristic Variation Propagation Analysis and Control in Product Development." *International Journal of Production Research* 51 (22): 6573–6593.

Gao, Xiang, Feng Hao, Daining Fang, and Zhuping Huang. 2013. "Boussinesq Problem with the Surface Effect and Its Application to Contact Mechanics at the Nanoscale." *International Journal of Solids and Structures* 50 (16-17): 2620–2630.

Genta, Gianfranco, Maurizio Galetto, and Fiorenzo Franceschini. 2018. "Product Complexity and Design of Inspection Strategies for Assembly Manufacturing Processes." *International Journal of Production Research* 56 (11): 4056–4066.

Guo, Junkang, Baotong Li, Zhigang Liu, Jun Hong, and Xiaopan Wu. 2016. "Integration of Geometric Variation and Part Deformation Into Variation Propagation of 3-D Assemblies." *International Journal of Production Research* 54 (19): 5708–5721.

Hoon Ko, Jeong, and Dong-Woo Cho. 2005. "3D Ball-end Milling Force Model Using Instantaneous Cutting Force Coefficients." *Journal of Manufacturing Science and Engineering* 127 (1): 1–12.

Hu, S. Jack, and Yoram Koren. 1997. "Stream-of-variation Theory for Automotive Body Assembly." *CIRP Annals* 46 (1): 1–6.

Huang, Qiang, Jianjun Shi, and Jingxia Yuan. 2003. "Part Dimensional Error and Its Propagation Modeling in Multi-Operational Machining Processes." *Journal of Manufacturing Science and Engineering* 125 (2): 255–262.

Jia, Zhiyang, and Liang Zhang. 2019. "Serial Production Lines with Geometric Machines and Finite Production Runs: Performance Analysis and System-Theoretic Properties." *International Journal of Production Research* 57 (8): 2247–2262.

Jin, Jionghua, and Jianjun Shi. 1999. "State Space Modeling of Sheet Metal Assembly for Dimensional Control." *Journal of Manufacturing Science and Engineering* 121 (4): 756–762.

Li, Guilong, Shichang Du, Delin Huang, Chen Zhao, and Yafei Deng. 2019. "Elastic Mechanics-Based Fixturing Scheme Optimization of Variable Stiffness Structure Workpieces for Surface Quality Improvement." *Precision Engineering* 56: 343–363.

Liu, Shihong, Shichang Du, and Lifeng Xi. 2018. "Transient Analysis of Quality Performance in Two-Stage Manufacturing Systems with Remote Quality Information Feedback." *Computers & Industrial Engineering* 117: 262–281.

Loose, Jean-Philippe, Shiyu Zhou, and Dariusz Ceglarek. 2007. "Kinematic Analysis of Dimensional Variation Propagation for Multistage Machining Processes with General Fixture Layouts." *IEEE Transactions on Automation Science and Engineering* 4 (2): 141–152.

Loose, Jean-Philippe, Qiang Zhou, Shiyu Zhou, and Darek Ceglarek. 2010. "Integrating GD&T into Dimensional Variation Models for Multistage Machining Processes." *International Journal of Production Research* 48 (11): 3129–3149.

Mantripragada, Ramakrishna, and Daniel E Whitney. 1999. "Modeling and Controlling Variation Propagation in Mechanical Assemblies Using State Transition Models." *IEEE Transactions on Robotics and Automation* 15 (1): 124–140.

Paul, Richard P. 1981. "Robot Manipulators: Mathematics, Programming, and Control: The Computer Control of Robot Manipulators: Richard Paul".

Rezaei-Malek, Mohammad, Mehrdad Mohammadi, Jean-Yves Dantan, Ali Siadat, and Reza Tavakkoli-Moghaddam. 2019b. "A Review on Optimisation of Part Quality Inspection Planning in a Multi-Stage Manufacturing System." *International Journal of Production Research* 57 (15–16): 4880–4897.

Rezaei-Malek, Mohammad, Ali Siadat, Jean-Yves Dantan, and Reza Tavakkoli-Moghaddam. 2019a. "A Trade-off Between Productivity and Cost for the Integrated Part Quality Inspection and Preventive Maintenance Planning under Uncertainty." *International Journal of Production Research* 57 (19): 5951–5973.

Shao, Yiping, Kun Wang, Shichang Du, and Lifeng Xi. 2018. "High Definition Metrology Enabled Three Dimensional Discontinuous Surface Filtering by Extended Tetrolet Transform." *Journal of Manufacturing Systems* 49: 75–92.

Shao, Yiping, Yaxiang Yin, Shichang Du, and Lifeng Xi. 2019. "A Surface Connectivity-Based Approach for Leakage Channel Prediction in Static Sealing Interface." *Journal of Tribology* 141 (6): 062201.

Shao, Yiping, Yaxiang Yin, Shichang Du, Tangbin Xia, and Lifeng Xi. 2018. "Leakage Monitoring in Static Sealing Interface Based on Three Dimensional Surface Topography Indicator." *Journal of Manufacturing Science and Engineering* 140 (10): 101003.

Shi, Jianjun. 2006. *Stream of Variation Modeling and Analysis for Multistage Manufacturing Processes*. New York: CRC press.

Shi, Jianjun, and Shiyu Zhou. 2009. "Quality Control and Improvement for Multistage Systems: A Survey." *Iie Transactions* 41 (9): 744–753.

Tang, Aijun, and Zhanqiang Liu. 2008. "Deformations of Thin-Walled Plate Due to Static End Milling Force." *Journal of Materials Processing Technology* 206 (1-3): 345–351.

Timoshenko, S. P., and J. N. Goodier. 1971. *Theory of Elasticity*. New York: McGraw-Hill Book.

Vasundara, M., and K. P. Padmanaban. 2014. "Recent Developments on Machining Fixture Layout Design, Analysis, and Optimization Using Finite Element Method and Evolutionary Techniques." *The International Journal of Advanced Manufacturing Technology* 70 (1-4): 79–96.

Wan, Min, Wenjie Pan, Weihong Zhang, Yingchao Ma, and Yun Yang. 2014. "A Unified Instantaneous Cutting Force Model for Flat end Mills with Variable Geometries." *Journal of Materials Processing Technology* 214 (3): 641–650.

Wan, Min, Wei-Hong Zhang, Jian-Wei Dang, and Yun Yang. 2009. "New Procedures for Calibration of Instantaneous Cutting Force Coefficients and Cutter Runout Parameters in Peripheral Milling." *International Journal of Machine Tools and Manufacture* 49 (14): 1144–1151.

Wang, Kun, Shichang Du, and Lifeng Xi. 2020. "Three-dimensional Tolerance Analysis Modelling of Variation Propagation in Multi-Stage Machining Processes for General Shape Workpieces." *International Journal of Precision Engineering and Manufacturing* 21 (1): 31–44.

Wang, Kun, Yaxiang Yin, Shichang Du, Lifeng Xi, and Tangbin Xia. 2017. "State Space Modeling of Multi-Scale Variation Propagation in Machining Process Using Matrix Model." Paper presented at the 2017 IEEE International Conference on Industrial Engineering and Engineering Management.

Yang, Fuyong, Sun Jin, and Zhimin Li. 2017a. "A Comprehensive Study of Linear Variation Propagation Modeling Methods for Multistage Machining Processes." *The International Journal of Advanced Manufacturing Technology* 90 (5-8): 2139–2151.

Yang, Fuyong, Sun Jin, and Zhimin Li. 2017b. "A Modification of DMVs Based State Space Model of Variation Propagation for Multistage Machining Processes." *Assembly Automation* 37 (4): 381–390.

Yanıkoğlu, İhsan, and Meltem Denizel. 2020. "The Value of Quality Grading in Remanufacturing under Quality Level Uncertainty." *International Journal of Production Research* 1–21. doi:10.1080/00207543.2020.1711983.

Yeh, Junghua, and Frank W Liou. 1999. "Contact Condition Modelling for Machining Fixture Setup Processes." *International Journal of Machine Tools and Manufacture* 39 (5): 787–803.

Yi, Sinan, Gengdong Cheng, and Liang Xu. 2016. "Stiffness Design of Heterogeneous Periodic Beam by Topology Optimization with Integration of Commercial Software." *Computers & Structures* 172: 71–80.

Yi, Sinan, Liang Xu, Gengdong Cheng, and Yuanwu Cai. 2015. "FEM Formulation of Homogenization Method for Effective Properties of Periodic Heterogeneous Beam and Size Effect of Basic Cell in Thickness Direction." *Computers & Structures* 156: 1–11.

Zhang, Hongying, Michael Yu Wang, Jisen Li, and Jian Zhu. 2016. "A Soft Compressive Sensor Using Dielectric Elastomers." *Smart Materials and Structures* 25 (3): 035045.

Zhao, Yixiao, Di Zhou Yihai He, Anqi Zhang, Xiao Han, Yao Li, and Wenzhuo Wang. 2020. "Functional Risk-Oriented Integrated Preventive Maintenance Considering Product Quality Loss for Multistate Manufacturing Systems." *International Journal of Production Research* 1–18. doi:10.1080/00207543.2020.1713416.

Zhou, Shiyu, Qiang Huang, and Jianjun Shi. 2003. "State Space Modeling of Dimensional Variation Propagation in Multistage Machining Process Using Differential Motion Vectors." *IEEE Transactions on Robotics and Automation* 19 (2): 296–309.

Appendix

Derivation of A_{mn} and B_{mn}, i.e. Equations (21) and (22):

Based on the orthogonality of trigonometric functions in Equation (A.1).

$$\int_0^{L_a/2} \sin\frac{m\pi x}{L_a} \sin\frac{m'\pi x}{L_a}\ \mathrm{d}x = \begin{cases} 0 & \text{for } m \neq m' \\ L_a/2 & \text{for } m = m' \end{cases} \tag{A.1}$$

Multiplying both sides of Equation (19) by $\sin(m\pi x/L_a)\sin(n\pi y/L_b)$, and integrating x and y in $[0, L_a]$ and $[0, L_b]$ respectively, the left side and right side of Equation (19) after conversion can be derived as

$$\begin{cases} \text{Left} = \int_0^{L_b} \int_0^{L_a} F(x,y) \sin\frac{m\pi x}{L_a} \sin\frac{n\pi y}{L_b}\ \mathrm{d}x\mathrm{d}y \\ \text{Right} = A_{mn} \cdot \int_0^{L_b} \int_0^{L_a} \sin\frac{m\pi x}{L_a} \sin\frac{m\pi x}{L_a} \sin\frac{n\pi y}{L_b} \sin\frac{n\pi y}{L_b}\ \mathrm{d}x\mathrm{d}y = A_{mn} \cdot \frac{L_a}{2} \cdot \frac{L_b}{2} \end{cases} \tag{A.2}$$

Therefore, the coefficient A_{mn} is

$$A_{mn} = \frac{4}{L_a L_b} \int_0^{L_b} \int_0^{L_a} F(x,y) \sin\frac{m\pi x}{L_a} \sin\frac{n\pi y}{L_b}\ \mathrm{d}x\mathrm{d}y \tag{A.3}$$

Substituting Equation (20) into the deflection Equation (17)

$$\pi^4 D \cdot \sum_{m=1}^{\infty} \sum_{n=1}^{\infty} \left(\frac{m^2}{L_a^2} + \frac{n^2}{L_b^2} \right) B_{mn} \sin \frac{m\pi x}{L_a} \sin \frac{n\pi y}{L_b} = F(x, y) \tag{A.4}$$

Then, substituting Equation (A.3) into Equation (19) and then further substituting into Equation (A.4)

$$\pi^4 D \cdot \sum_{m=1}^{\infty} \sum_{n=1}^{\infty} \left(\frac{m^2}{L_a^2} + \frac{n^2}{L_b^2} \right) B_{mn} \sin \frac{m\pi x}{L_a} \sin \frac{n\pi y}{L_b} = \sum_{m=1}^{\infty} \sum_{n=1}^{\infty} A_{mn} \sin \frac{m\pi x}{L_a} \sin \frac{n\pi y}{L_b} \tag{A.5}$$

For any $\{(x, y) | 0 < x < L_a, 0 < y < L_b\}$, coefficients of the trigonometric series on both sides of Equation (A.5) should be correspondingly equal, thus

$$B_{mn} = \frac{A_{mn}}{\pi^4 D \cdot ((m^2/L_a^2) + (n^2/L_b^2))} = \frac{4 \int_0^{L_b} \int_0^{L_a} F(x, y) \sin(m\pi x/L_a) \sin(n\pi y/L_b) dx dy}{\pi^4 D \cdot L_a L_b \cdot ((m^2/L_a^2) + (n^2/L_b^2))} \tag{A.6}$$